



# The HELINOIR Aeroacoustic Code and its Application to Active/Passive Helicopter Noise Reduction

Miang H. Chia\*, Karthikeyan Duraisamy†, Ashwani K. Padthe‡ and Peretz P. Friedmann§

*University of Michigan, Ann Arbor, Michigan, 48109-2140, USA*

A suite of computational tools capable of predicting in-plane low frequency rotorcraft noise and its control using blade tip geometry modifications is developed. The combined code, consisting of AVINOR, a comprehensive rotorcraft analysis code, and an acoustic code called HELINOIR, is first validated against wind tunnel tests, and subsequently verified against computational results. A rotor configuration resembling the MBB BO105 with a swept tip was simulated for level flight at a moderate advance ratio. The impact of passive blade geometry modification on in-plane noise and vibration was studied and compared to the in-plane noise reduction obtained using a single 20% chord active plain trailing edge flap with a feedback microphone on the left boom. In-plane noise below the horizon was reduced using active control whereas it was amplified using passive control. There is a vibration performance tradeoff associated with in-plane noise reduction.

## Nomenclature

|              |   |
|--------------|---|
| $a_0$        | Speed of sound  |
| $c$          | Rotor blade chord   |
| $[C]$        | Damping matrix  |
| $C_{df}$     | Fuselage drag coefficient                                     |
| $C_W$        | Helicopter weight coefficient                                 |
| $C_T$        | Thrust coefficient  |
| $e$          | Blade root offset from center of rotation                     |
| $\mathbf{F}$ | Load vector in the equation of motion                         |
| $J$          | Quadratic cost function                                       |
| $[K]$        | Stiffness matrix  |
| $l_i$        | Sectional load in the $i$ direction                           |
| $L_b$        | Non dimensional blade length                                  |
| $[M]$        | Mass matrix   |
| $M_b$        | Mass of one blade   |
| $M_i$        | Mach number of source in the $i$ direction                    |
| $N_b$        | Number of rotor blades  |
| $p$          | Acoustic pressure   |
| $\mathbf{Q}$ | Weighting matrix for plant output                             |
| $r$          | Distance from source to observer                              |
| $R$          | Rotor blade radius  |
| $\mathbf{R}$ | Weighting on the control input                                |
| $\mathbf{T}$ | Sensitivity matrix relating control input to the plant output |
| $\mathbf{u}$ | Control input vector  |
| $v_n$        | Wall normal velocity at blade surface                         |
| $\mathbf{w}$ | Disturbance vector  |

\*PhD Candidate, Department of Aerospace Engineering, and AIAA Student Member.

†Assistant Professor of Aerospace Engineering, Department of Aerospace Engineering, and AIAA Member.

‡Research Investigator, Department of Aerospace Engineering, and AIAA Member.

§François-Xavier Bagnoud Professor of Aerospace Engineering, Department of Aerospace Engineering, and AIAA Fellow.

|                  |   |
|------------------|---|
| <b>W</b>         | Matrix relating plant response to disturbance   |
| $\vec{x}$        | Observer location   |
| $X_A$            | Offset between the aerodynamic center and the elastic axis                            |
| $X_{Ib}$         | Offset of the blade cross-sectional center of mass from the elastic axis              |
| $X_{FA}, Z_{FA}$ | Longitudinal and vertical offsets between rotor hub and helicopter aerodynamic center |
| $X_{FC}, Z_{FC}$ | Longitudinal and vertical offsets between rotor hub and helicopter center of gravity  |
| <b>y</b>         | State vector for the coupled aeroelastic model  |
| <b>z</b>         | Plant output vector   |

*Subscript*

|       |                 |
|-------|-----------------|
| $i,j$ | Variable number |
| $L$   | Loading noise   |
| $ret$ | Retarded time   |
| $T$   | Thickness noise |

*Symbols*

|                                |   |
|--------------------------------|---|
| $\alpha_D$                     | Descent angle                                     |
| $\alpha_R$                     | Rotor shaft angle                                 |
| $\beta_p$                      | Blade precone angle                               |
| $\gamma$                       | Lock number                                       |
| $\Delta S$                     | Surface area of panel                             |
| $\phi_R$                       | Lateral roll angle                                |
| $\mu$                          | Advance ratio                                     |
| $\rho_0$                       | Air density                                       |
| $\theta_0$                     | Collective pitch                                  |
| $\theta_{0t}$                  | Tail rotor pitch angle                            |
| $\theta_{1c}, \theta_{1s}$     | Cyclic pitch components                           |
| $\theta_{tw}$                  | Blade pretwist distribution                       |
| $\sigma$                       | Rotor solidity                                    |
| $\omega_F, \omega_L, \omega_T$ | Blade flap, lag and torsional natural frequencies |
| $\Omega$                       | Rotor angular speed                               |
| $\psi$                         | Azimuth angle                                     |

## I. Introduction

THE acoustic environment of a rotorcraft is complex. Figure 1 shows the different components of helicopter noise and the associated directivity. The dominance of each component varies with flight condition. The out-of-plane Blade Vortex Interaction (BVI) noise, which is dominant in a low-speed descending flight, can severely limit a civilian helicopter's community acceptance. In-plane, low-frequency rotorcraft noise is of particular concern from a military operation standpoint as it tends to propagate for long distances without significant attenuation, adversely affecting the aural detection range of a rotorcraft, and hence its operational survivability. Helicopter noise suppression has been studied using passive means based on rotor blade geometry design modifications, mainly in the outboard 10% of the blade span, as well as active control methods.

Typical passive control methods consist of blade tip planform modifications such as sweep, anhedral, dihedral, etc. For BVI noise, blade tip shapes that produce vortex diffusion, e.g. Ogee tip, have been shown to be effective (Ref. 2). Blade sweep is also effective in reducing BVI noise by avoiding or delaying parallel interactions between the blade and the vortices (Ref. 3). For in-plane noise, thinning and tapering the tip of the rotor blade reduces the thickness noise contribution (Ref. 4). At high rotor tip speed, sweeping the blade reduces the effects of compressibility, effectively delaying delocalization and the onset of HSI noise (Ref. 5). However, the contribution of blade sweep at moderate tip speed is less clear. It was shown in Ref. 6 that the sweep angle is not an important parameter, as compared to the taper ratio, as the sweep angle affects the quadrupole noise, which is not dominant at moderate tip speed. On the other hand, it was shown in Ref. 7 that the sweep angle introduces a phase shift effect between spanwise distributed source and sink couples, resulting in in-plane noise reduction. Despite the valuable insights gained, these studies had limitations as

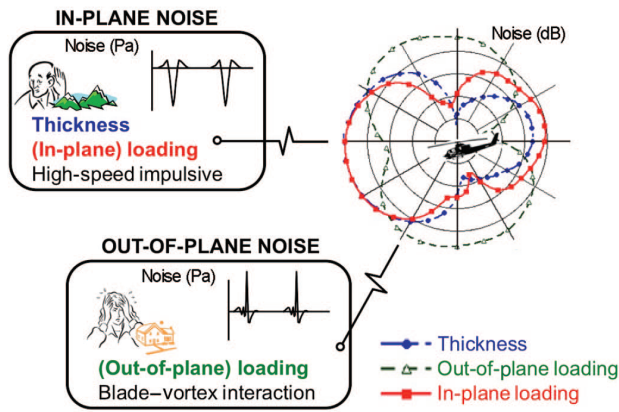


**Figure 1.** Rotor noise components and directivity characteristics. (From Ref. 1)

some of them were purely CFD based aerodynamic studies while the rest used simplistic structural dynamic models (Ref. 8). This is particularly problematic for swept and anhedral tips as they introduce strong bending torsion coupling, influencing blade vibrations and aeroelastic stability. Furthermore, these studies have not explored the adverse effects of noise reduction on the hub vibratory loads. In order to accurately predict the helicopter noise and the effects of its suppression on the vibratory loads, it is essential to account for blade deflections and rotor trim using a high fidelity rotor aeroelastic model coupled with an aeroacoustic model.

Several active control approaches such as higher harmonic control (HHC), pitch link actuated individual blade control (IBC), and on-blade control (OBC) implemented through a trailing edge flap or a microflap have been studied for noise control (Ref. 9). These techniques modify the blade airloads in order to influence the BVI interactions for BVI noise reduction (Ref. 4) or to generate an “anti-noise” signal for in-plane noise reduction (Ref. 1). However, implementation of active control on a production helicopter has an associated cost which needs to be justified by sufficient benefits. Therefore, it is important to compare the noise reduction performance of the active approaches to other techniques such as passive blade geometry modification. The primary goal of this paper is to describe the HELIcopter NOIse Reduction (HELINOIR) (Ref. 10) aeroacoustic code, and use it for both active and passive noise reduction. The impact of the noise suppression on the vibratory loads will also be examined.

An accurate computational study of active/passive noise control and its influence on the hub vibrations requires a high-fidelity aeroelastic/aeroacoustic code that is also computationally efficient. The HELINOIR code combined with the Active VIbration and NOise Reduction (AVINOR) comprehensive rotorcraft analysis code (Ref. 11) is well suited for such a study. The AVINOR code coupled with HELINOIR has been validated for out-of-plane BVI and in-plane noise prediction and verified for active in-plane noise control using an active flap (Ref. 12). The AVINOR/HELINOIR code is further developed in the current study to examine passive noise reduction using modified blade tip planforms. The specific objectives of the paper are:

1. Provide a detailed description of the HELINOIR code.
2. Describe the combined AVINOR/HELINOIR aeroelastic-aeroacoustic computational framework, including the tip planform and geometry modifications.
3. Use the aeroelastic-aeroacoustic framework for passive noise control while accounting for the potential vibration impact.
4. Compare performance of the passive methods to that of active on-blade control methods.

## II. Description of the the Acoustic Methodology and HELINOIR Code

The aeroacoustic computations are based on the solution of the Ffowcs-Williams and Hawkings (Ref. 13) equations, using the Farassat 1A formulation (Ref. 14, 15). In this work, monopole and dipole sources of

noise are considered, corresponding to the thickness and loading noise, respectively. Quadrupole, or volume noise sources that arise due to phenomena such as shockwaves and separated flows, are neglected. For the problems of interest in this work, it is reasonable to expect that quadrupole noise sources are relatively unimportant as loading and thickness noise sources.

The Farassat 1A formulation for the acoustic pressure from thickness ( $p_T$ ) and loading ( $p_L$ ) noise sources at an observer locations  $\vec{x}$  and time  $t$  is given by the following:

$$\begin{aligned} p_T(\vec{x}, t) &= \frac{1}{4\pi} \sum_j \left[ \frac{\rho_o \dot{v}_n}{r(1 - M_r)^2} \right]_{ret,j} \Delta S_j + \\ &\quad \frac{1}{4\pi} \sum_j \left[ \frac{\rho_o v_n (r \dot{M} \hat{r}_i + a_o M_r - a_o M^2)}{r^2 (1 - M_r)^3} \right]_{ret,j} \Delta S_j, \end{aligned} \quad (1)$$

$$\begin{aligned} p_L(\vec{x}, t) &= \frac{1}{4\pi a_o} \sum_j \left[ \frac{\dot{l}_i \hat{r}_i}{r(1 - M_r)^2} \right]_{ret,j} \Delta S_j + \\ &\quad \frac{1}{4\pi} \sum_j \left[ \frac{l_i \hat{r}_i - l_i M_i}{r^2 (1 - M_r)^2} \right]_{ret,j} \Delta S_j + \\ &\quad \frac{1}{4\pi a_o} \sum_j \left[ \frac{l_r (r \dot{M}_i \hat{r}_i + a_o M_r - a_o M^2)}{r^2 (1 - M_r)^3} \right]_{ret,j} \Delta S_j. \end{aligned} \quad (2)$$

The blade is discretized into a number of flat panels of surface area  $\Delta S_j$  and the contribution of each panel  $j$  to the noise is recorded in retarded time (subscript  $ret$ ) and interpolated to the desired observer time.

In Equations (1) and (2),  $\rho_o, a_o$  represent the ambient density and speed of sound, respectively.  $v_n$  is the velocity of the quarter-chord point of the panel, projected in a direction normal to the airfoil camber.  $l_i$  is the sectional load in the  $i$  direction,  $M_i$  is the Mach number of the source in the  $i$  direction,  $r$  is the distance from the source to the observer and  $\hat{r} = r/|r|$ .  $(\cdot)$  denotes the rate of change of the quantity  $(\cdot)$  with respect to source time.

As conceptualized by Schmitz (Ref. 16), the forward section of an airfoil displaces fluid outwards and acts as a pressure source, while the aft part of the aerofoil acts as a pressure sink; this is illustrated in Fig. 2. In this work, the mass displacement is represented by a single source at  $x/c = 1/8$  and a single sink at  $x/c = 5/8$  for each airfoil section. The sectional loads are assumed to be point forces collocated at  $x/c = 1/4$ .

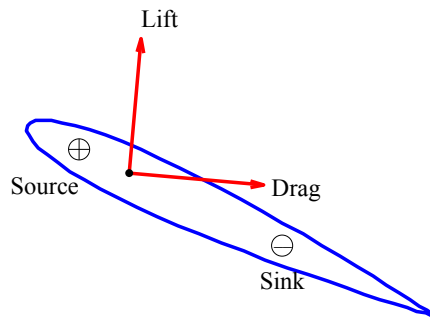


**Figure 2.** Source/sink representation for thickness noise generation.

This compact acoustic model is a reasonable approximation for far-field noise calculations because the distance of the observer from the noise source, is typically more than an order of magnitude larger than the blade chord. Extensive validation studies of thickness and loading noise signatures (Ref. 17, 18, 10, 19) have been performed with this model. To further demonstrate and verify the accuracy of this formulation, the

compact chord model presented above is compared to a version that uses the full blade pressure distributions and geometry obtained from a Computational Fluid Dynamics-based solution. The configuration used was the UH60 rotor in high-speed forward flight (Ref. 20) (advance ratio  $\mu = 0.3$ ,  $M_{tip} = 0.63$ ). Figure 3 shows a sample solution where the observer is located three rotor radii in front of the rotor plane, confirming the good agreement between the compact loading and full geometry models.

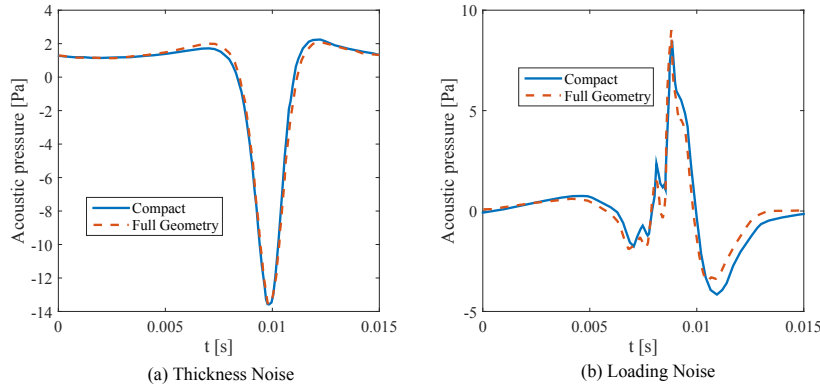


**Figure 3.** Verification of the compact model acoustic pressure predictions for a UH60 rotor at  $\mu=0.30$ ,  $M_{tip}=0.63$ , at an observer located 3R in front of the rotor plane.

### III. Brief Review of the AVINOR Code

Passive/active control simulations are performed using the Active VIbration and NOise Reduction (AVINOR) comprehensive rotorcraft analysis code, which consists of: (1) a structural dynamic model that can represent a rotor blade undergoing moderate deflections with coupled flap-lag-torsional dynamics, (2) a non-linear unsteady CFD based reduced order model (ROM) (Ref. 21) that captures the sectional aerodynamic loads accurately and (3) a control model suitable for noise and vibration reduction. The code has been validated in previous studies (Refs. 9, 22). The principal features of AVINOR are summarized next.

#### A. Structural dynamic model

The rotor is modeled as a four-bladed hingeless rotor, with fully coupled flap-lag-torsional dynamics for each blade. Two different structural models are used in this comparative study, a Galerkin type finite element model for the rotor blade with swept tip for passive control and a global Galerkin model for the straight blade with an OBC device for active control.

##### 1. Galerkin Type Finite Element Model

The finite element model is based on an analysis developed by Yuan and Friedmann (Ref. 23, 24), which is capable of modeling blades with transverse shear deformations, cross sectional warping, and swept tips. The equations of motion are formulated using a finite element discretization of Hamilton's principle, with the assumption that the blade undergoes moderate deflections. The beam-type finite elements used for the discretization have 23 nodal degrees of freedom. In this study, modal reduction employing eight normal modes, namely the first three flap modes, first two lead-lag modes, first two torsional modes, and the first axial mode, are used to reduce the number of structural degrees of freedom.

##### 2. Global Galerkin Model

For active control, the isotropic blade model is used. The rotor blade is modeled as a slender cantilever beam composed of a linearly elastic homogeneous material undergoing moderate deflections. The structural dynamic equations are discretized using the global Galerkin method, employing three flap, two lead-lag, and two torsional free vibration modes of the rotating blade. Each rotating mode is obtained from nine non-rotating uniform beam modes. The effect of control surfaces on the structural properties of the blade is

neglected. Thus, the control surfaces influence blade behavior only through their effect on the aerodynamic and inertial loads. This structural model is computationally more efficient compared to the finite element model, especially when coupled with OBC devices.

## B. Aerodynamic model

The blade/plain flap sectional aerodynamic loads for attached flow are calculated using a computational fluid dynamics (CFD) based reduced order model (ROM) (Ref. 22). The ROM is based on rational function approximations (RFA) representing a least squares fit to the aerodynamic load response data obtained using CFD simulations. This model accurately predicts the unsteady aerodynamic lift, moment, and drag forces while taking a fraction of computational time compared to CFD. Accounting for both unsteady lift and drag forces is critical for accurate in-plane noise prediction. For the swept tip region, the chordwise component of the freestream flow velocity experienced at the swept blade section is used to determine the unsteady aerodynamic loads. The ROM model is linked to a free wake model (Ref. 25) that yields a spanwise and azimuthally varying inflow distribution. For the separated flow regime, the aerodynamic loads are obtained using the ONERA dynamic stall model (Ref. 26).

## C. Coupled aeroelastic response/trim solution

For the passive control study, the equation of motion for the blade representing an equilibrium between the inertia, aerodynamic and structural loads is discretized using a finite element approach. The finite element degrees of freedom are reduced by a normal mode transformation using coupled free vibration modes of the rotating blade. This process results in a system of coupled nonlinear differential equation with periodic coefficients written as

$$[M(\mathbf{y})]\ddot{\mathbf{y}} + [C(\mathbf{y}, \dot{\mathbf{y}})] + [K(\mathbf{y}, \dot{\mathbf{y}}, \ddot{\mathbf{y}})]\mathbf{y} + \mathbf{F}(\mathbf{y}, \dot{\mathbf{y}}, \ddot{\mathbf{y}}) = 0 \quad (3)$$

This system of equations is cast into the first-order state variable form and integrated in the time domain using the Adams-Basforth predictor corrector algorithm. Two different trim procedures were used. For the validation studies, a wind tunnel trim procedure, where only the three moment equations are enforced, is used to replicate the test conditions. A propulsive trim procedure, where three force equations (longitudinal, lateral, and vertical) and three moment equations (roll, pitch, and yaw) are enforced, was employed in the verification studies and final results. The trim equations are solved in a coupled manner with the aeroelastic equations of motions, Eqn. 3. A simplified tail rotor model, based on uniform inflow and blade element theory, is used. The six trim variables are the rotor shaft angle  $\alpha_R$ , the collective pitch  $\theta_0$ , the cyclic pitch  $\theta_{1s}$  and  $\theta_{1c}$ , the tail rotor constant pitch  $\theta_{0t}$ , and lateral roll angle  $\phi_R$ . The vibratory hub shears, and moments are calculated by integrating the distributed inertial and aerodynamic loads over the entire blade span in the rotating frame, then transforming these loads to the hub fixed nonrotating system, and summing the contributions from each blade.

## D. The Higher Harmonic Control Algorithm

Active control of vibration and noise in this study is implemented using the adaptive HHC algorithm (Refs. 27, 21). This algorithm is based on the assumption that the helicopter can be represented by a linear model relating the output of interest  $\mathbf{z}$  to the control input  $\mathbf{u}$ . The measurement of the plant output and update of the control input are performed at specific times  $t_k = k\tau$ , where  $\tau$  is the time interval between updates during which the plant output reaches a steady state. In actual implementation of the algorithm, this time interval may be one or more revolutions. A schematic of the HHC architecture implemented on a helicopter is shown in Fig. 4.

The disturbance  $\mathbf{w}$  represents the helicopter operating condition. The output vector at the  $k^{th}$  time step is given by

$$\mathbf{z}_k = \mathbf{T}\mathbf{u}_k + \mathbf{W}\mathbf{w} \quad (4)$$

where the sensitivity matrix  $\mathbf{T}$  represents a linear approximation of the helicopter response to the control and is given by

$$\mathbf{T} = \frac{\partial \mathbf{z}}{\partial \mathbf{u}}. \quad (5)$$

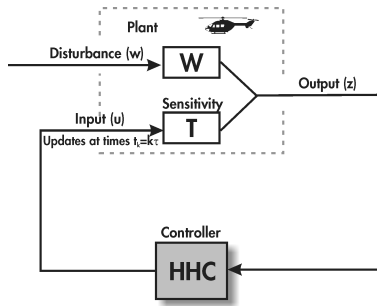


**Figure 4.** Higher harmonic control architecture

The controller is based on the minimization of a general quadratic cost function

$$J(\mathbf{z}_k, \mathbf{u}_k) = \mathbf{z}_k^T \mathbf{Q} \mathbf{z}_k + \mathbf{u}_k^T \mathbf{R} \mathbf{u}_k. \quad (6)$$

The optimal control input is determined from the requirement

$$\frac{\partial J(\mathbf{z}_k, \mathbf{u}_k)}{\partial \mathbf{u}_k} = 0, \quad (7)$$

which yields the optimal control law  $\mathbf{u}_{k,\text{opt}}$ , given by

$$\mathbf{u}_{k,\text{opt}} = -(\mathbf{T}^T \mathbf{Q} \mathbf{T} + \mathbf{R})^{-1} (\mathbf{T}^T \mathbf{Q}) (\mathbf{z}_0 - \mathbf{T} \mathbf{u}_0). \quad (8)$$

This is the classical version of the HHC algorithm that yields an explicit relation for the optimal control input. An adaptive version of the HHC algorithm has been shown to perform better than the classical HHC when the model nonlinearities are significant and the sensitivity matrix  $\mathbf{T}$  is a poor approximation of the model (Ref. 27). In the adaptive HHC algorithm, the sensitivity matrix  $\mathbf{T}$  is updated recursively, based on the input and output history, using a least-squares methods. A detailed description of this version is provided in Ref. 27 and the details of its implementation for active in-plane noise control is provided in Ref. 12.

#### IV. The Aeroelastic-Aeroacoustic Framework

The data flow between the AVINOR and HELINOIR code is shown in Fig. 5 for the case of active on-blade control. A set of coupled trim/aeroelastic equations is solved in AVINOR to determine the blade aeroelastic response and aerodynamic loading at each time step. The blade position, velocities, and the aerodynamic loads are passed on to the HELINOIR code for acoustic computation. To ensure data consistency between AVINOR and HELINOIR, a series of coordinate transformations and re-dimesionalization is performed. The HELINOIR code computes the acoustic pressure, using the blade loads and kinematic data obtained from AVINOR, as a post processing step. For closed loop active noise control, HELINOIR computes the acoustic pressure at the feedback location, which is sent back to the Higher Harmonic Controller (HHC). The HHC computes the OBC inputs that minimize a quadratic cost function based on the feedback microphone noise levels as well as the control input magnitudes. For passive control, a similar framework is used except that the feedback loop with the HHC is not used.

#### V. Validation Studies

The AVINOR/HELINOIR code, employing a straight blade modelled using the global Galerkin method, has been validated against experimental data (Ref. 12) obtained in two major wind tunnel tests: 1) the Higher-harmonic-control Aeroacoustic Rotor Test (HART) (Ref. 28) and 2) the Boeing-SMART rotor wind tunnel test conducted in the 40'x80' Wind Tunnel at the NASA Ames Research Center (Ref. 29).

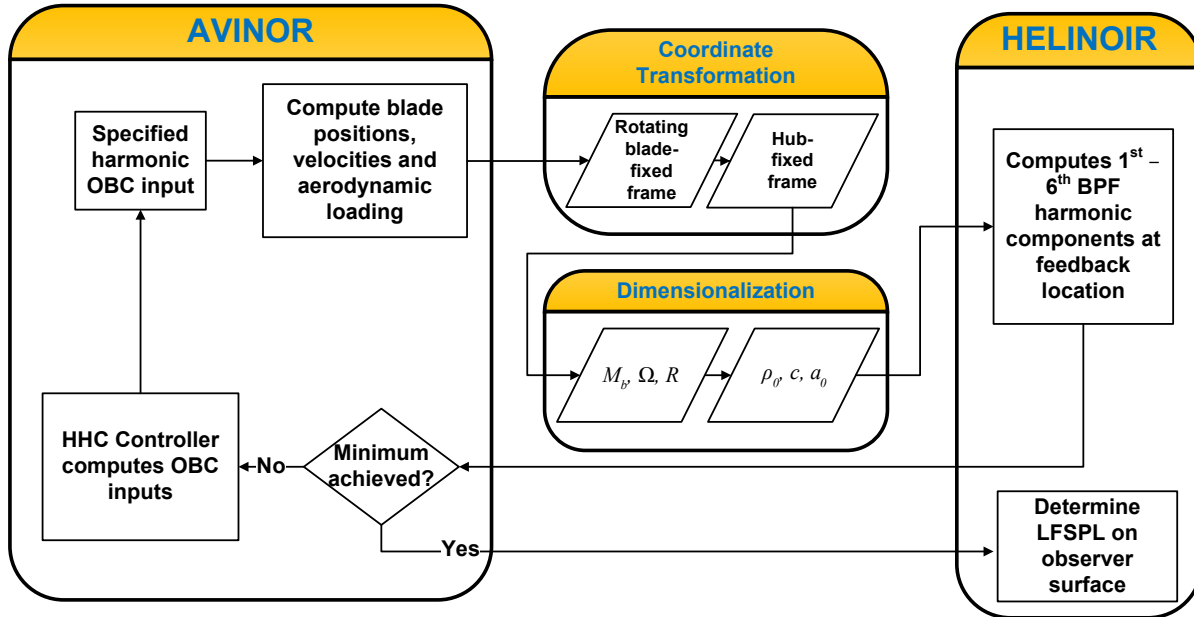


Figure 5. Data flowchart between AVINOR and HELINOIR for active control.

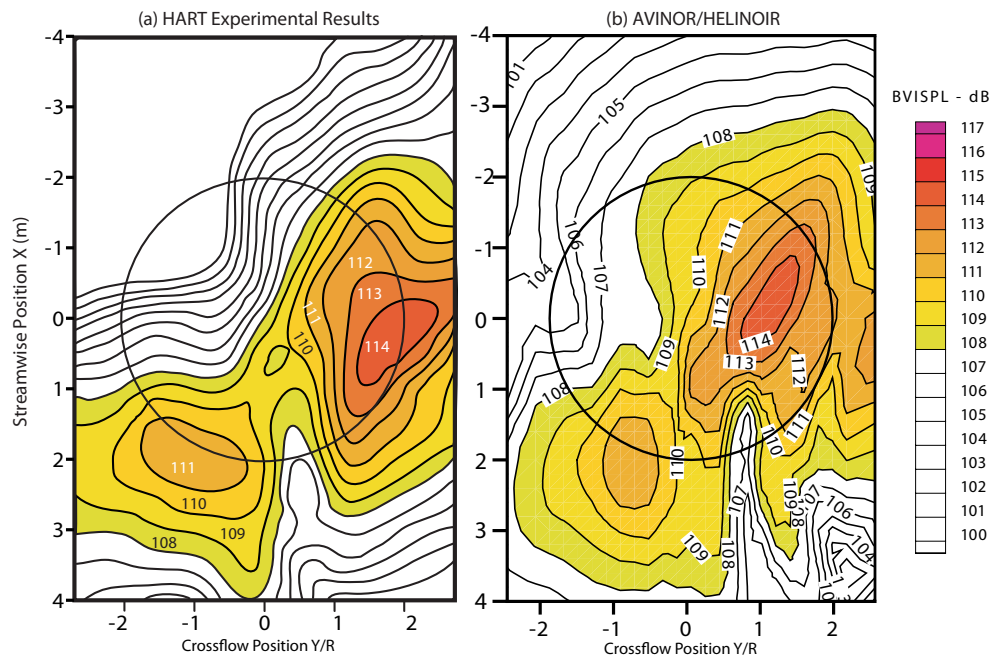
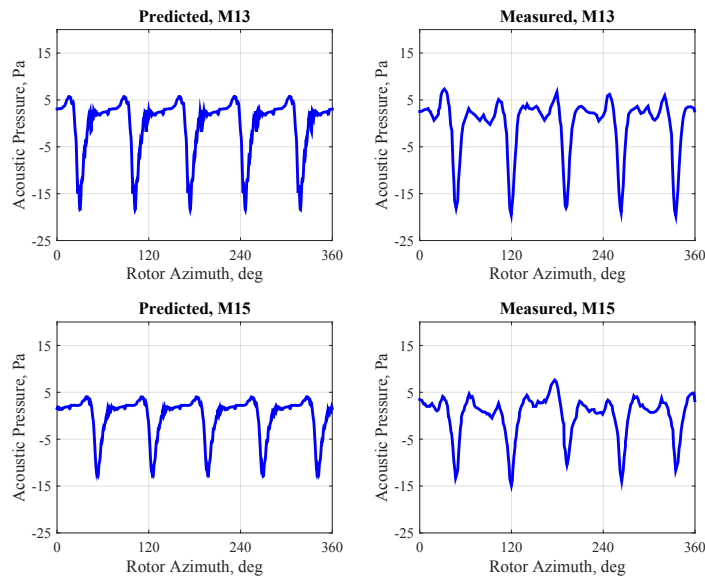


Figure 6. Validation of the acoustic computations against the HART experimental data.

For the HART validation, the baseline flight condition corresponds to a heavy BVI descending flight, with  $\mu=0.15$ ,  $C_T = 0.044$  and  $\alpha_D = 6.5^\circ$ . The HART rotor is a 40% dynamically and Mach-scaled model of a 4-bladed hingeless MBB BO-105 main rotor. The BVI Sound Pressure Levels (BVISPL) were measured on a carpet plane positioned 1.15R below the rotor hub and parallel to the hub plane. The noise levels from the experiment are shown in Fig. 6(a) and the results from the simulation with AVINOR/HELINOIR are

shown in Fig. 6(b). The new code predicts the BVI noise levels on the carpet plane very well, capturing the magnitude and location of the noise peaks of 114 dB on the advancing side and 111 dB on the retreating side accurately.

For the Boeing-SMART Rotor validation, the baseline flight condition was level cruise, at  $\mu = 0.30$  and  $C_T = 0.006$ . The SMART rotor is a full scale, bearingless five bladed main rotor modified from an MD900 Explorer rotor system. For the code validation, the structural properties of the blade model were chosen to match the first modal frequencies,  $\omega_{L1}, \omega_{F1}, \omega_{T1}$ , of the SMART rotor (Ref. 30), following the procedure described in Ref. 31. Three in-plane microphones (M13, M15 and M14), positioned along a straight line originating from the advancing blade tip to the tunnel centerline, were used for low frequency, in-plane noise measurements. The predicted and measured acoustic pressure histories at the M13 and M15 microphones are shown in Fig. 7, and it is evident that the pressure history is predicted well, capturing the peak-to-peak amplitude accurately. Further details of the code validation and verification can be found in Ref. 12.



**Figure 7.** Validation of the acoustic computations against the Boeing SMART experimental data. (Experimental data from Ref. 1)

## VI. Verification Studies

In order to model the advanced tip geometry used in passive control, a beam type finite element model of a rotor blade, based on the analysis in Ref. 24, was implemented in AVINOR/HELINOIR as part of this study. To verify the new structural model, the acoustic and vibration calculations are compared against the results from the AVINOR/WOPWOP code (Ref. 31) based on the global Galerkin method.

A helicopter configuration resembling a full-scale four bladed MBB BO-105 hingeless rotor is used. The rotor parameters are listed in Table 1 (Ref. 32). All the values in the table (except  $C_W$ ,  $\gamma$ , and  $\sigma$ ) have been nondimensionalized using  $M_b$ ,  $R$ , and  $1/\Omega$  for mass, length and time, respectively. Constant mass and stiffness distributions are assumed along the blade span. Using these parameters, it was found that six beam-type finite elements are needed to match the modal frequencies,  $\omega_{Fi}, \omega_{Li}, \omega_{Ti}$  used in the global Galerkin model. The baseline flight condition is a descending flight at an advance ratio  $\mu = 0.15$ , thrust coefficient  $C_T = 0.005$ , and descent angle  $\alpha_D = 6.5^\circ$ , representing heavy BVI conditions. The acoustic environment represented by BVISPL computed on a carpet plane located 1.15R beneath the rotor is compared in these verification studies.

The baseline noise level on the carpet plane computed using the AVINOR/WOPWOP code employing the global Galerkin model is shown in Fig. 8(a). Results from simulations performed using the FEM AVINOR code in combination with WOPWOP and HELINOIR are shown in Figs. 8(b) and (c), respectively. It is

**Table 1.** Baseline rotor parameters.

| <u>Dimensional Rotor Data</u>    |                           |
|----------------------------------|---------------------------|
| $R = 4.91$ m                     |                           |
| $M_b = 27.35$ kg                 |                           |
| $\Omega = 425$ RPM               |                           |
| <u>Nondimensional Rotor Data</u> |                           |
| $N_b = 4$                        | $L_b = 1.0$               |
| $c/R = 0.05498$                  | $\theta_{tw} = -8^\circ$  |
| $e = 0$                          |                           |
| $X_A = 0$                        | $X_{Ib} = 0$              |
| $\omega_F = 1.124, 3.40, 7.60$   | $\omega_L = 0.732, 4.458$ |
| $\omega_T = 3.17, 9.08$          |                           |
| $\gamma = 5.5$                   | $\sigma = 0.07$           |
| $\beta_p = 2.5^\circ$            |                           |
| <u>Helicopter Data</u>           |                           |
| $C_W = 0.005$                    | $C_{df} = 0.031$          |
| $X_{FA} = 0.0$                   | $Z_{FA} = 0.3$            |
| $X_{FC} = 0.0$                   | $Z_{FC} = 0.3$            |

evident that the finite element model, whether it is coupled with WOPWOP or HELINOIR, predicts the BVI noise levels on the carpet plane well, capturing the magnitude and location of the noise peaks of 114dB on the advancing side and 111dB on the retreating side.

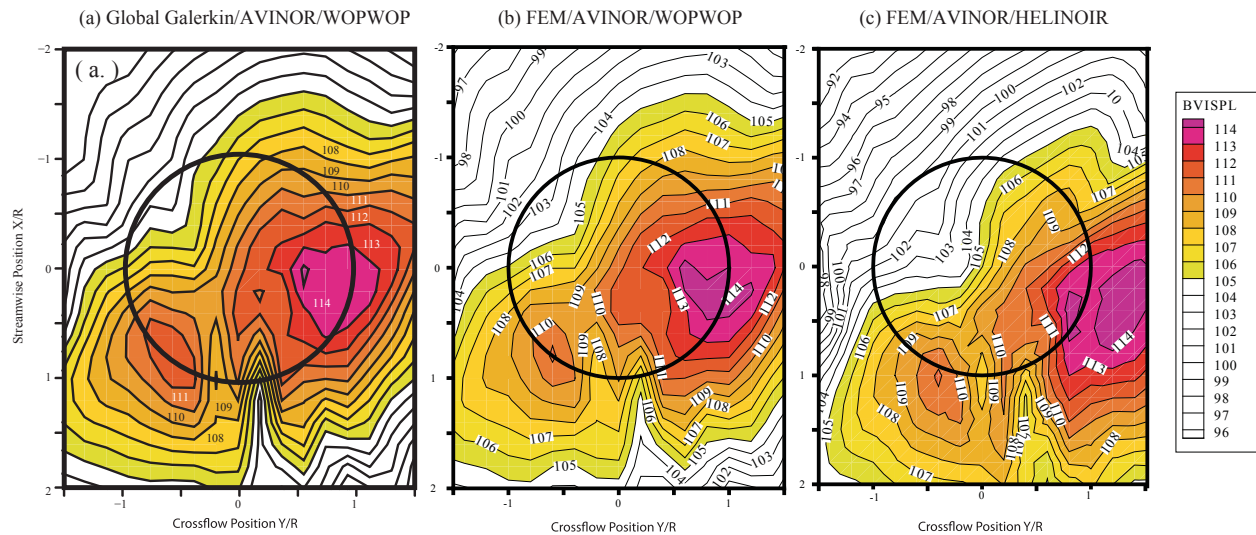


**Figure 8.** Comparison of the noise levels from a straight blade computed on the carpet plane employing a global Galerkin model (a) and Galerkin type FEM (b) and (c) at  $\mu = 0.15$ ,  $C_T = 0.005$  and  $\alpha_D = 6.5^\circ$

The associated baseline 4/rev non-dimensional vibratory hub loads for the three code combinations are shown in Fig. 9. There is good agreement in all six components of the vibratory hub loads. It is evident that both the acoustic and vibratory load predictions from the finite element structural model, coupled with HELINOIR agrees well with the global Galerkin AVINOR/WOPWOP code combination.

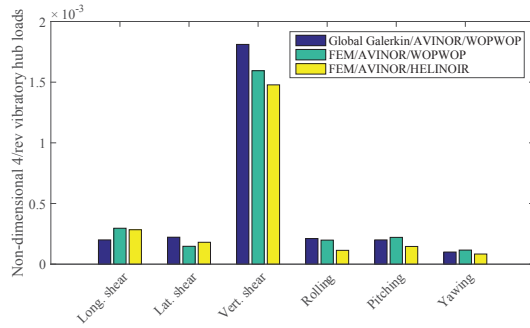


**Figure 9.** Comparison of the vibration levels from a baseline blade employing a global Galerkin model and Galerkin type FEM at  $\mu = 0.15$ ,  $C_T = 0.005$  and  $\alpha_D = 6.5^\circ$

## VII. Results and Discussion

The simulation results presented in this section are for a helicopter resembling a full-scale 4-bladed MBB BO-105 hingeless rotor in level flight at an advance ratio,  $\mu = 0.3$ . The baseline rotor parameters are provided in Table 1. The rotor is trimmed using propulsive trim.

Passive in-plane noise control is implemented through a swept tip geometry spanning 10% of the blade. The orientation of the swept tip relative to the straight portion is described by a sweep angle  $\Lambda_s$  and is defined positive backward, as shown in Fig. 10. The blade is modeled by a series of six beam-type finite elements along the elastic axis. Five elements are used to model the straight segment of the blade which spans 90% of the blade length, and the swept tip is modeled using a single finite element. Sweep angles up to a maximum of  $6^\circ$  were considered.

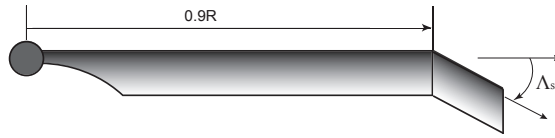


**Figure 10.** Rotor blade with a swept tip geometry.

Passive control results are compared against active control results obtained using a 20% $c$  plain flap, shown in Fig. 11. A single flap configuration is used, shown in Fig. 12. The single flap has a span of  $0.12R$  and is centered at  $0.75R$ . The rotor blade in the active control case is modeled as a slender beam cantilevered at the hub.

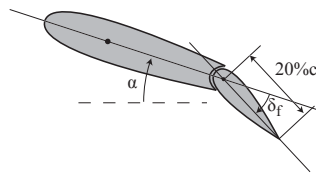


**Figure 11.** On-blade control device used in the study.

It was found in Ref 12 that a microphone located on the left boom position provided the best feedback for closed loop in-plane noise reduction. The feedback microphone location is illustrated in Fig. 13.

The far-field acoustic environment in front of the helicopter is characterized by Low Frequency Sound Pressure Level (LFSPL), consisting of the 1st - 6th blade passage frequency (BPF) harmonic components of the rotor noise which are the principal components of in-plane low frequency noise (Ref. 1). The LFSPL is computed on a spherical segment located at a distance of  $10R$  in front of the rotor hub, with an azimuth angle between  $135^\circ$  to  $225^\circ$  and an elevation angle between  $-90^\circ$  to  $15^\circ$ , as shown in Fig. 14. This surface includes the observer locations in the forward in-plane direction where noise reduction is considered.

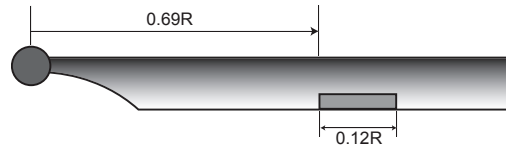


**Figure 12.** Single flap configuration of the plain flap on the rotor blade.

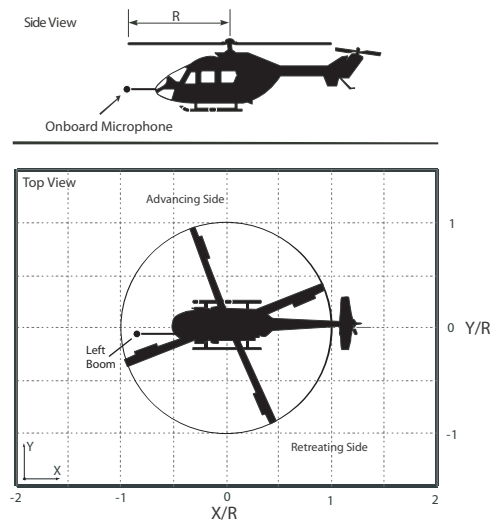


**Figure 13.** Near-field onboard microphone feedback location on left boom and tip of the right skid.

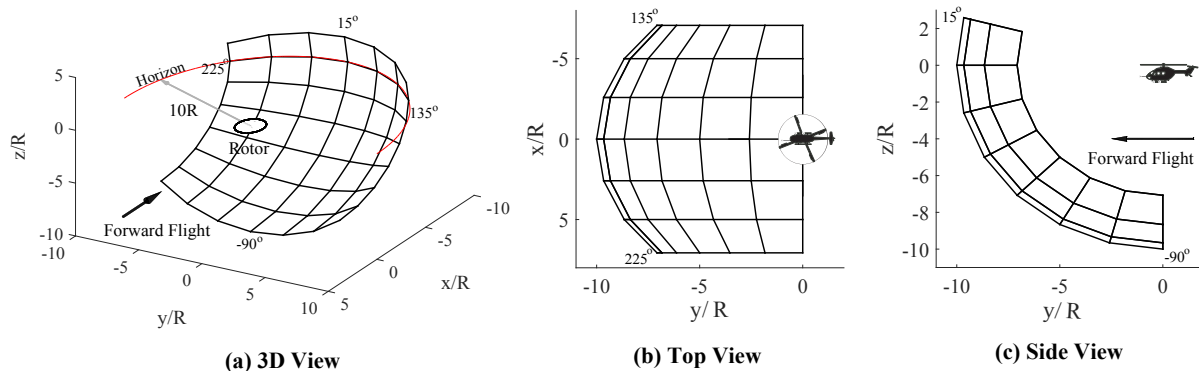
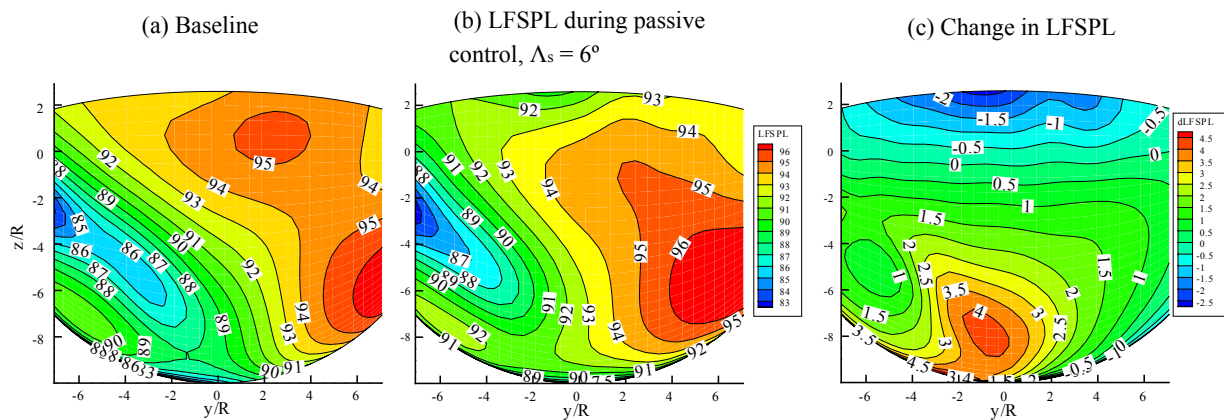


**Figure 14.** In plane observer surface located at 10R in front of the helicopter. Azimuthal variation is shown in (b) and in elevation is shown in (c).

## A. Noise Reduction Using Passive Control

The baseline LFSPL noise obtained using the finite-element based AVINOR/HELINOR code combination is shown in Fig. 15(a). Two regions of high noise levels, above 95dB, are predicted in front of the rotor, at around  $(\frac{y}{R}, \frac{z}{R}) = (2, 0)$  and  $(\frac{y}{R}, \frac{z}{R}) = (-7, 6)$ . It is this directivity and the low frequency content of the LFSPL noise that increases the range at which the helicopter can be detected in forward flight.

The LFSPL obtained using a rotor blade with swept tip,  $\Lambda_s = 6^\circ$ , is shown in Fig. 15(b). The change in the LFSPL from the baseline is shown in Fig. 15(c). There is no significant change in the LFSPL in the in-plane direction on the horizon,  $\frac{z}{R} = 0$  or  $0^\circ$  elevation angle. Therefore the swept tip does not contribute significantly to the in-plane noise on the horizon at moderate tip speed when quadrupole noise is not significant. This result is in agreement with Ref. 6. However, the swept tip also introduces a noise reduction of up to 2 dB above the horizon,  $\frac{z}{R} = 2$  or  $15^\circ$  elevation angle and more significantly a noise increase of up to 4dB below the horizon,  $\frac{z}{R} = -7$  or  $-45^\circ$  elevation angle. This increase in the LFSPL noise below the horizon increases the range at which rotorcraft can be detected and is not desirable.



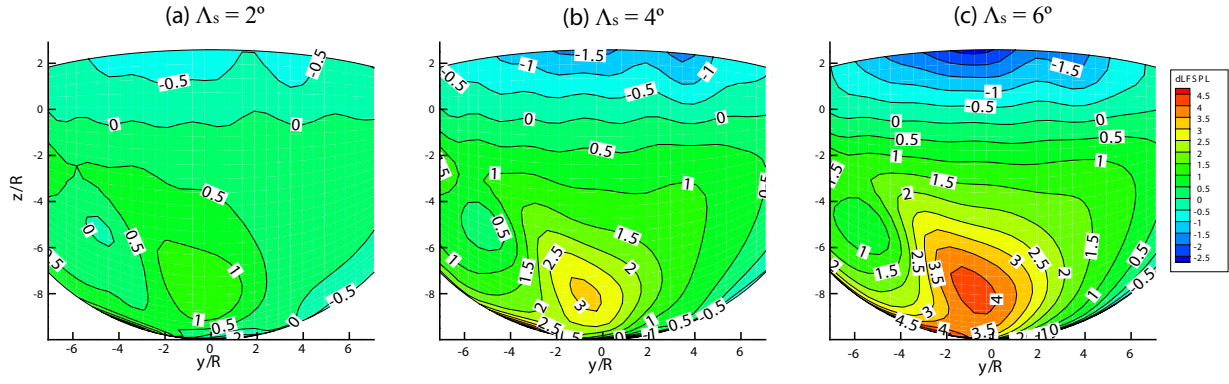
**Figure 15.** Baseline and the in-plane noise levels obtained using a swept tip,  $\Lambda = 6^\circ$ , on the observer surface at  $10R$ .

Figure 16 shows the effect of the variation of sweep angle on the in-plane noise and Fig 17 shows the associated 4/rev vibratory hub loads. It is evident that increasing the sweep angle increases the LFSPL noise below the horizon and therefore the range at which a helicopter can be detected. However, this is accompanied by a reduction in the vibratory hub loads, particularly the 4/rev vertical hub shear. For a sweep angle,  $\Lambda_s = 6^\circ$ , the vertical hub shear was reduced by up to 32%. The reduction in the vibratory vertical hub shear, with the introduction of a swept tip is consistent with the findings in Ref. 33 and is attributed to the redistribution of unsteady aerodynamic loading as a result of the dynamic response of the blade.

The reason behind in-plane noise increase below the horizon can be better understood by examining the acoustic pressure history at an in-plane observer location of a rotor blade with and without a swept tip. Figures 18(a) and 18(b) show the acoustic pressure history for the baseline blade and the blade with a swept tip,  $\Lambda_s = 6^\circ$ , at the observer location,  $(\frac{x}{R}, \frac{y}{R}, \frac{z}{R}) = (-9.70, -0.27, -2.41)$ . This observer location corresponds to the forward, slight downward tilt of the main rotor tip path plane and is significant for determining the range at which the helicopter can be detected and is the point where maximum LFSPL reduction is achieved using active control (Ref. 12). By comparing Figs. 18(a) and (b), there is a marginal reduction in the thickness noise. However, this reduction in thickness noise is offset by an increase in loading noise resulting in an overall increase in the total acoustic pressure and in-plane noise below the horizon.

## B. Noise Reduction Using Active Control

The baseline LFSPL noise, without active control is shown in Fig. 19(a). A region of high noise levels, above 95dB, is predicted around  $(\frac{y}{R}, \frac{z}{R}) = (0, 0)$  that is, at  $0^\circ$  elevation angle and  $180^\circ$  azimuth angle. This baseline is similar to that predicted using the finite element model shown in Fig. 15(a).



**Figure 16.** Increase in the LFSPL noise below the horizon obtained at  $10R$  for different sweep angles at  $\mu = 0.3$ .

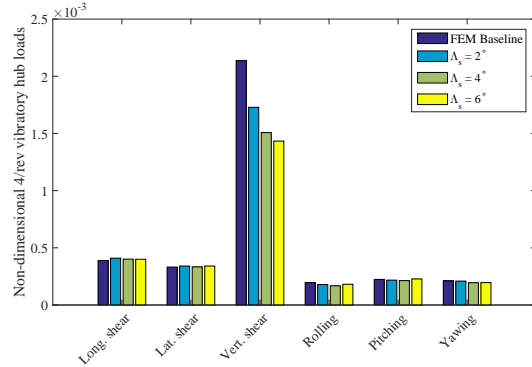


**Figure 17.** Vibration levels for different sweep angles at  $\mu = 0.3$

The LFSPL noise reduction obtained using a single plain flap with a single near-field feedback microphone on the left boom is shown Fig. 19(b). The change in LFSPL from the baseline is shown in Fig. 19(c). It can be seen that significant noise reduction of up to 6dB was achieved between  $-4 \leq \frac{y}{R} \leq 4$ ,  $-4 \leq \frac{z}{R} \leq -1$  or an elevation angle of between  $-23^\circ$  to  $4^\circ$  from the horizon and azimuth angle between  $156^\circ$  to  $204^\circ$ . This direction corresponds to the forward, slight downward tilt of the main rotor tip path plane and is the most significant for reducing the range at which the helicopter can be detected. However, a noise increase of up to 18 dB is generated in the left, out-of-plane location. This suggests that the reduction of in-plane noise using active control can result in a severe noise penalty in the out-of-plane direction.

The vibration levels obtained during active in-plane noise control using the single plain flap are compared to the baseline levels in Fig. 20. It is evident that a vibration penalty is induced during in-plane noise reduction for all the six 4/rev vibratory hub load components, with a maximum increase of 60.6% in the vertical hub shear.

### C. Comparison Between Passive and Active Control

By comparing the change in LFSPL due to passive control using a swept tip,  $\Lambda_s = 6^\circ$ , Fig. 15(c), and active control using a single plain flap, Fig. 19(c), it can be seen that the reduction of in-plane LFSPL below the horizon, can best be achieved using active control where a reduction of up to 6dB was achieved. On the other hand, there is an increase of up to 4dB in LFSPL below the horizon when passive control is used. In both cases, there is a LFSPL increase in the out-of-plane direction, suggesting that any noise control approaches may have to be further optimized so that the noise reduction performance gain in one direction is not compromised by the noise amplification in other directions.

It should be noted that there is a trade-off between in-plane noise reduction performance and vibration

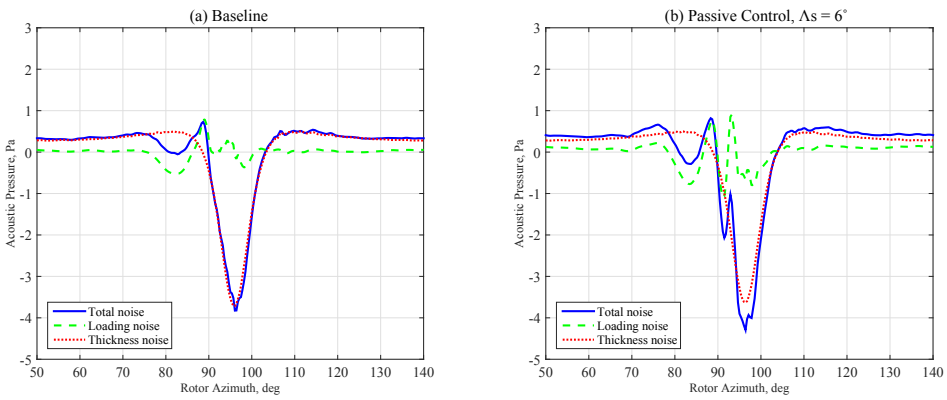


**Figure 18.** Acoustic pressure histories at observer location  $(\frac{x}{R}, \frac{y}{R}, \frac{z}{R}) = (-9.70, -0.27, -2.41)$  with baseline blade (a) and swept tip blade (b).

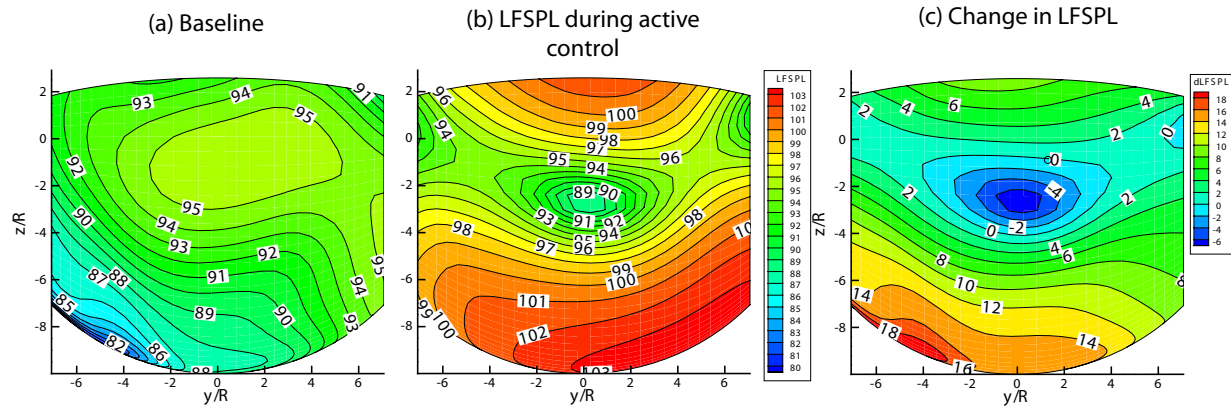


**Figure 19.** Baseline and the reduced in-plane noise levels obtained using active control, implemented using a single plain flap and a nose boom feedback, for an MBB BO105 rotor during level flight,  $\mu = 0.30$ .

levels. In-plane LFSPL reduction achieved below the horizon using active OBC is accompanied by an increase in vibratory hubload, Fig. 20, whereas in-plane LFSPL increase below the horizon using passive control is accompanied by a decrease in the vibratory hub load, Fig. 17.

The loading noise plays a critical role in in-plane noise reduction/amplification, even though the negative peak pressure generated by the thickness noise is the dominant contributor to the in-plane noise. In the case of a swept tip blade, Fig. 18, the total noise increased due to the in-phase increase in loading noise, while the thickness noise was reduced marginally. On the other hand, if an anti-phase loading noise had been generated, e.g. by active control (Ref. 12), it would cancel the dominant negative peak thickness noise to reduce the total in-plane noise.

## VIII. Conclusions

The AVINOR code, employing a CFD-based unsteady reduced order aerodynamic model, was coupled with a noise prediction code named HELINOIR. The acoustic calculations were based on a compact loading model which takes into account both the airfoil lift and drag forces. The compact loading model was separately verified for accuracy against a pressure distribution model obtained from CFD. Acoustic predictions for this code combination were validated against the HART and Boeing SMART Rotor experimental results. A Galerkin type finite element model was subsequently developed for AVINOR/HELINOIR. This new code combination was verified against BVI noise results obtained using the AVINOR/WOPWOP. The compar-

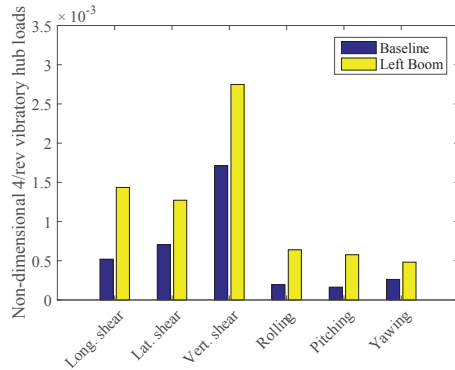


**Figure 20. Vibration penalty during in-plane noise reduction using a single plain flap with a nose boom feedback.**

isons show that the new code is capable of producing accurate in-plane and out-of-plane noise predictions.

The new AVINOR/HELINOIR code was used for in-plane LFSPL noise prediction for level flight at moderate advance ratio. Both active and passive control methods were studied. Passive control was implemented through a swept tip. Active control was implemented through a conventional plain flap with a feedback microphone mounted on the left boom of the helicopter. The impact of both control approaches on in-plane LFSPL noise and vibration were examined and compared. The principal conclusions of the study are summarized below.

1. The acoustic predictions from AVINOR/HELINOIR were validated against experimental results from the HART I and Boeing SMART Rotor programs. For the HART rotor validation, the BVISPL on a carpet plane located 1.15R below the rotor hub during a descending flight at  $\mu = 0.15$ ,  $C_T = 0.0044$ , and  $\alpha_D = 6.5^\circ$ , was accurately predicted by the code. For the Boeing SMART Rotor validation, LFSPL at the in-plane microphones, M13 and M15, during level flight at  $\mu = 0.3$  and  $C_T = 0.006$ , was also predicted accurately by the code.
2. The compact acoustic model used in the HELINOIR code gives an efficient and accurate prediction for far-field in-plane noise calculations compared to the full pressure distribution and geometry model obtained from CFD.
3. A Galerkin type finite element model for the MBB BO105 rotor was implemented in AVINOR/HELINOIR and verified against AVINOR/WOPWOP. The baseline BVI noise and vibration of a MBB BO105 rotor at  $\mu = 0.15$ ,  $C_T = 0.005$  and  $\alpha_D = 6.5^\circ$  predicted by AVINOR/HELINOIR were similar to those from AVINOR/WOPWOP.
4. Passive control, implemented through a swept tip of  $\Lambda_s = 6^\circ$  on a MBB BO105 rotor, results in a in-plane LFSPL noise reduction of up to 2dB above the horizon and an LFSPL increase of up to 4dB below the horizon at a moderate advance ratio,  $\mu = 0.3$ . There is no change in the in-plane LFSPL on the horizon. The increase in the LFSPL below the horizon increases the range at which a helicopter can be detected and is not desirable.
5. A swept tip reduces the vibratory hub loads for a helicopter in level flight,  $\mu = 0.3$ . A sweep angle of  $\Lambda_s = 6^\circ$  reduces the 4/rev vertical hub shear amplitude by up to 32%.
6. Active closed-loop in-plane noise reduction of up to 6dB was obtained below the horizon with plain flaps using the feedback microphone located at the left boom tip. However, this in-plane noise reduction was accompanied by a concurrent out-of-plane noise increase of up to 18dB.
7. There is a vibration penalty associated with active in-plane noise reduction below the horizon. The increase in 4/rev vertical hub shear amplitude was about 60% during in-plane noise reduction using the single plain flap. Therefore, there is a trade-off between in-plane noise reduction below the horizon and vibration performance.

8. The thickness noise component, which is the principal contributor to in-plane noise, is not altered significantly by the passive or active control methods studied. Controlling the loading noise component is key to the reduction of in-plane LFSPL noise.

## Acknowledgments

This work was supported in part by the FXB Center for Rotary and Fixed Wing Air Vehicle Design (FXB-CRFWAD).

## References

- <sup>1</sup>Sim, B. W., JanakiRam, R. D., and Lau, B. H., "Reduced In-Plane, Low-Frequency Noise of an Active Flap Rotor," *Journal of the American Helicopter Society*, Vol. 59, No. 2, April 2014, pp. 1–17.
- <sup>2</sup>Landgrebe, A. J. and Bellinger, E., "Experimental Investigation of Model Variable - Geometry and Ogee-Tip Rotors," Tech. Rep. CR-2275, NASA, Feb 1974.
- <sup>3</sup>Yu, Y. H., "Rotor Blade-Vortex Interaction Noise," *Progress in Aerospace Sciences*, Vol. 36, No. 2, Feb. 2000, pp. 97–115.
- <sup>4</sup>Conner, D. A. and Hoad, D. R., *Reduction of High-Speed Impulsive Noise by Blade Planform Modification of a Model Helicopter Rotor*, NASA TM84553, 1982.
- <sup>5</sup>Baeder, J., "Passive Design for Reduction of High-Speed Impulsive Rotor Noise," *Journal of the American Helicopter Society*, Vol. 43(3), Jul 1998, pp. 222–234.
- <sup>6</sup>Lyrantzis, A., Jameson, J., and Koutsavdis, E., "Technical Note: A Study of Rotorcraft Blade-Tip Shape High Speed Impulsive Noise Characteristics," *Journal of the American Helicopter Society*, Vol. 45(1), Jan 2000, pp. 54–57.
- <sup>7</sup>Prieur, J., Lafon, P., Caplot, M., and Desopper, A., "Aerodynamics and Acoustics of Rectangular and Swept Rotor Blade Tips," *Journal of the American Helicopter Society*, Vol. 34(1), Jan 1989, pp. 42–51.
- <sup>8</sup>Brocklehurst, A. and Barakos, G., "A Review of Helicopter Rotor Blade Tip Shapes," *Progress in Aerospace Sciences*, Vol. 56, Jan 2013, pp. 35–74.
- <sup>9</sup>Friedmann, P. P., "On-Blade Control of Rotor Vibration, Noise and Vibration: Just Around the Corner? The 33rd Alexander Nikolsky Honorary Lecture," *Journal of American Helicopter Society*, Vol. 59, No. 4, Oct. 2014, pp. 8–21.
- <sup>10</sup>Kim, H. W., Duraisamy, K., and Brown, R. E., "Effect of Rotor Stiffness and Lift Offset on the Aeroacoustics of a Coaxial Rotor in Level Flight," *Proceedings of the 65th American Helicopter Society Annual Forum*, May 2009.
- <sup>11</sup>Glaz, B., Goel, T., Liu, L., Friedmann, P. P., and Haftka, R. T., "Multiple-Surrogate Approach to Helicopter Rotor Blade Vibration Reduction," *AIAA Journal*, Vol. 47, No. 1, January 2009, pp. 271–282.
- <sup>12</sup>Chia, M., Padthe, A., Duraisamy, K., and Friedmann, P., "An Efficient Approach for the Simulation and On-Blade Control of Noise and Vibration," *Proceedings of the 72nd American Helicopter Society Annual Forum*, May 2016.
- <sup>13</sup>Ffowcs Williams, J. E. and Hawkings, D. L., "Sound Generation by Turbulence and Surfaces in Arbitrary Motion," *Philosophical Transactions of Royal Soc. London, Series A*, Vol. 264, No. 1151, May 1969, pp. 321–342.
- <sup>14</sup>Farassat, F. and Succi, G. P., "A Review of Propeller Discrete Frequency Noise Prediction Technology with Emphasis on Two Current Methods for Time Domain Calculations," *Journal of Sound and Vibration*, Vol. 71, No. 3, 1980.
- <sup>15</sup>Farassat, F. and Succi, G., "The Prediction of Helicopter Rotor Discrete Frequency Noise," *Vertica*, Vol. 7, No. 4, Oct. 1983, pp. 309–320.
- <sup>16</sup>Schmitz, F. H., *Rotor Noise, Aeroacoustics of Flight Vehicles, Vol.1: Noise Sources*, NASA Technical Report 90-3052, Aug 1991.
- <sup>17</sup>Kelly, M. E., Duraisamy, K., and Brown, R. E., "Predicting Blade Vortex Interaction, Airloads and Acoustics Using the Vorticity Transport Model," *Proceedings of the AHS Specialist's Conference on Aeromechanics*, January 2008.
- <sup>18</sup>Thom, A. and Duraisamy, K., "High Resolution Simulations of Parallel Blade-Vortex Interactions," *AIAA Journal*, Vol. 48, No. 10, October 2010.
- <sup>19</sup>Kim, H., Kenyon, A., Brown, R., and Duraisamy, K., "Interactional Aerodynamics and Acoustics of a Hingeless Coaxial Helicopter with an Auxiliary Propeller in Forward Flight," *The Aeronautical Journal*, Vol. 113, No. 1140, February 2009, pp. 65–78.
- <sup>20</sup>Lorber, P., "Aerodynamic Results of Pressure-Instrumented Model Rotor Test at the DNW," *Journal of American Helicopter Society*, Vol. 36, No. 4, 1991, pp. 66–76.
- <sup>21</sup>Padthe, A. and Friedmann, P. P., "Simultaneous Blade-Vortex Interaction Noise and Vibration Reduction in Rotorcraft Using Microflaps, Including the Effect of Actuator Saturation," *Journal of American Helicopter Society*, Vol. 60, No. 4, October 2015, pp. 1–16.
- <sup>22</sup>Liu, L., Padthe, A. K., and Friedmann, P. P., "Computational Study of Microflaps with Application to Vibration Reduction in Helicopter Rotors," *AIAA Journal*, Vol. 49, No. 7, July 2011, pp. 1450–1465.
- <sup>23</sup>Yuan, K. A. and Friedmann, P., "Structural Optimization for Vibratory Loads Reduction of Composite Helicopter Rotor Blades with Advanced Geometry Tips," *Journal of the American Helicopter Society*, Vol. 43, No. (3), July 1998, pp. 246–256.
- <sup>24</sup>Yuan, K. A. and Friedmann, P. P., *Aeroelastic and Structural Optimization of Composite Helicopter Rotor Blades with Swept Tips*, NASA CR 4665, June 1995.
- <sup>25</sup>Patt, D., Liu, L., and Friedmann, P. P., "Simultaneous Vibration and Noise Reduction in Rotorcraft Using Aeroelastic Simulation," *Journal of the American Helicopter Society*, Vol. 51, No. 2, April 2006, pp. 127–140.
- <sup>26</sup>Petot, D., "Differential Equation Modeling of Dynamic Stall," *La Recherche Aérospatiale*, Vol. 5, 1989, pp. 59–71.

<sup>27</sup>Patt, D., Liu, L., Chandrasekar, J., Bernstein, D. S., and Friedmann, P. P., "Higher-Harmonic-Control Algorithm for Helicopter Vibration Reduction Revisited," *Journal of Guidance, Control, and Dynamics*, Vol. 28, No. 5, September-October 2005, pp. 918–930.

<sup>28</sup>Splettstoesser, W., Seelhorst, U., Wagner, W., Boutier, A., Micheli, F., Mercker, E., and Pengel, K., "Higher Harmonic Control Aeroacoustic Rotor Test (HART) - Test Documentation and Representative Results," Report IB 129-95/28 and appendices, DLR, Dec. 1995.

<sup>29</sup>Straub, F. K., Anand, V. R., Birchette, T. S., and Lau, B. H., "SMART Rotor Development and Wind Tunnel Test," *Proceedings of the 35th European Rotorcraft Forum*, Hamburg, Germany, Sep 2009.

<sup>30</sup>Straub, F. K., Anand, V., Birchette, T. S., and Lau, B. H., "Wind Tunnel Test of the SMART Active Flap Rotor," *Proceedings of the 65th American Helicopter Society Annual Forum*, May 2009.

<sup>31</sup>Liu, L., *BVI Induced Vibration and Noise Alleviation By Active and Passive Approaches*, Ph.D. thesis, University of Michigan, Ann Arbor, 2005.

<sup>32</sup>Padthe, A. K., Friedmann, P. P., Chia, M. H., and Liu, L., "A Comprehensive Numerical Assessment of Microflaps for On-Blade Control of Rotorcraft Noise and Vibration," *Journal of Aircraft*, Published online.

<sup>33</sup>de Terlizzi, M. and Friedmann, P. P., "Active Control of BVI Induced Vibrations Using a Refined Aerodynamic Model and Experimental Correlation," *American Helicopter Society 55th Annual Forum Proceedings*, Montreal, Canada, May 25-27 1999, pp. 599–615.